



Electrical Measurement of the Direct Spin Hall Effect in Fe/In_xGa_{1-x}As Heterostructures

E. S. Garlid,¹ Q. O. Hu,² M. K. Chan,¹ C. J. Palmström,^{2,3} and P. A. Crowell¹

¹*School of Physics and Astronomy, University of Minnesota, Minneapolis, Minnesota 55455, USA*

²*Department of Electrical and Computer Engineering, University of California, Santa Barbara, California 93106, USA*

³*Department of Materials, University of California, Santa Barbara, California 93106, USA*

(Received 26 May 2010; published 4 October 2010)

We report on an all-electrical measurement of the spin Hall effect in epitaxial Fe/In_xGa_{1-x}As heterostructures with *n*-type (Si) channel doping and highly doped Schottky tunnel barriers. A transverse spin current generated by an ordinary charge current flowing in the In_xGa_{1-x}As is detected by measuring the spin accumulation at the edges of the channel. The spin accumulation is identified through the observation of a Hanle effect in the voltage measured by pairs of ferromagnetic Hall contacts. We investigate the bias and temperature dependence of the resulting Hanle signal and determine the skew and side-jump contributions to the total spin Hall conductivity.

DOI: [10.1103/PhysRevLett.105.156602](https://doi.org/10.1103/PhysRevLett.105.156602)

PACS numbers: 72.25.Dc, 72.25.Rb, 85.75.-d

There has been extensive theoretical discussion of the spin Hall effect (SHE) in semiconductors, which is the coupling of charge and spin currents by spin-orbit interactions resulting from either charged impurities (extrinsic SHE) [1] or band structure (intrinsic SHE) [2], as well as of the various ways that the SHE could be exploited to generate or manipulate spin currents [3–8]. However, only a handful of recent experiments have investigated this effect, and for the extrinsic case in semiconductor materials they have relied on optical techniques to either detect [9–13] or generate [14] spins. The scope of experimental studies could be broadened significantly by access to transport techniques that can probe materials and device geometries which are not accessible optically.

We report on transport measurements of the SHE in lateral devices fabricated from Fe/In_xGa_{1-x}As heterostructures. The SHE is due to spin-orbit scattering of an ordinary charge current by impurities, resulting in a transverse spin current. In the geometry shown in Fig. 1(a), a charge current $j_x = \sigma_{xx}E_x$ flows down a channel of conductivity σ_{xx} in the presence of an electric field E_x . The electrons have a drift momentum $\hbar\mathbf{k} = (m^*j_x/ne)\hat{x}$, where n is the carrier density and m^* is the effective mass. The electron spins interact with impurities via the spin-orbit Hamiltonian $H_{so} = \lambda_{so}\boldsymbol{\sigma} \cdot (\mathbf{k} \times \nabla V)$, where λ_{so} is the spin-orbit coupling constant, $\boldsymbol{\sigma}$ is the Pauli spin operator, and V is the Coulomb-like scattering potential. The scattering leads to spin-dependent deflection of electrons, resulting in a spin current j_s perpendicular to both their spin orientation and drift momentum. This is the *extrinsic* spin Hall effect and is distinct from the intrinsic mechanisms present in systems with unusual band structures [15]. In steady state, the SHE leads to an accumulation of spins of opposite sign at the two edges of the channel, which we detect using Fe contacts as spin-dependent voltage probes. For the geometry shown in Fig. 1(a), we are sensitive to a spin current j_s that flows in the *y* direction, with the spin

oriented along *z*. We find that the magnitude of the spin Hall conductivity $\sigma_{SH} = j_s/E$ is in agreement with models of the extrinsic SHE due to ionized impurity scattering [5,7]. By analyzing the dependence of the SH signal on channel conductivity, we determine the relative magnitudes of the skew and side-jump contributions to the total spin Hall conductivity.

Epitaxial (001) Fe/In_xGa_{1-x}As heterostructures were grown by molecular beam epitaxy. The semiconductor epilayers were prepared as described in Ref. [16], and the active layers consist of a 2.5 μm thick Si-doped ($n = 3\text{--}5 \times 10^{16} \text{ cm}^{-3}$) channel, a highly doped Schottky tunnel barrier ($n^+ = 5 \times 10^{18} \text{ cm}^{-3}$), and a 5 nm thick Fe layer. Four heterostructures with In concentrations $x = 0.00, 0.03, 0.05,$ and 0.06 were studied. The wafers were subtractively processed into devices using standard lithographic and etching techniques [16]. Multiple devices were fabricated on a single chip with 30 μm wide channels oriented along the [110] direction, which is the *x* direction in the micrograph of Fig. 1(a). Pairs of Fe electrodes, each of which is 4 μm wide, were patterned so that the centers of the contacts in each pair are 2, 6, or 10 μm from the edges of the channel. Charge current injection contacts are located at the ends of the channel, $>250 \mu\text{m}$ away from the Fe contacts and out of the field of this image. The charge current j_x is therefore unpolarized. The spins are separated by the spin Hall effect, and we measure the voltage V_{ab} between the two Fe contacts, which are connected to pads by long Au vias that pass over a SiN isolation layer. A second set of contacts, indicated *c* and *d* in Fig. 1(a), are positioned on GaAs side arms. The voltage V_{cd} is used as a reference, and the difference $V_{ab} - V_{cd}$ comprises the measured signal. This differential measurement reduces the background Hall voltages, particularly a large hysteretic component ($\sim 50 \mu\text{V}$) that is due to the local magnetic fields generated by the Fe contacts.

Typical spin valve and Hanle effect curves (see Ref. [16] for a discussion) on a lateral spin valve device (fabricated

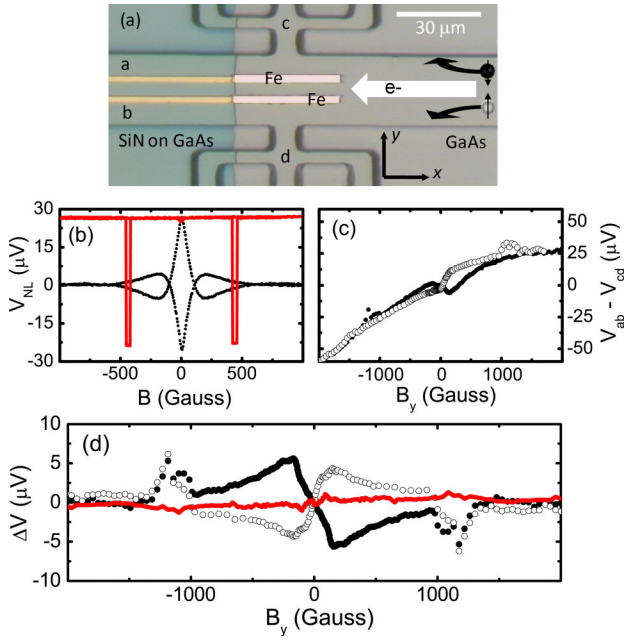


FIG. 1 (color online). (a) Micrograph of a spin Hall device with Fe contacts located $10 \mu\text{m}$ from the edges of the GaAs channel. The devices with contacts closer to the edges have a third contact in the center of the channel that is not used in this experiment. The contact pairs ab and cd are used to measure the spin accumulation. (b) Nonlocal spin valve (—) and Hanle effect (●) data obtained on a GaAs device at $T = 60 \text{ K}$ for $j_{\text{Inj}} = 8.2 \times 10^2 \text{ A/cm}^2$. Hanle data are shown for both parallel and antiparallel states of injector and detector. (c) The measured voltage $V_{ab} - V_{cd}$ for a GaAs device with Fe contacts $2 \mu\text{m}$ from the edges at $T = 30 \text{ K}$ for $j_x = 5.7 \times 10^3 \text{ A/cm}^2$ in the two different parallel states ($\uparrow\uparrow$, ●) and ($\downarrow\downarrow$, ○). An offset voltage of 13.2 mV has been subtracted from both sets of data. (d) The same data after extraction of the spin Hall signal for both positive (●) and negative (○) currents. The spin Hall signal in the antiparallel state is shown as the solid line.

from the same wafer, but with only a series of contacts across the channel) are shown in Fig. 1(b). These data establish that the ferromagnetic (FM) contacts are sensitive to the spin polarization generated by spin injection into the channel as well as its dephasing by precession in a magnetic field applied in the z direction. The Fe contacts, which have a strong easy axis along $[110]$, show sharp and reproducible switching behavior as well as nearly perfect remanence.

Since the contacts are magnetized along $[110]$ (\hat{x}), and the spin polarization generated by the spin Hall effect is oriented along $[001]$ (\hat{z}), a field B_y is applied to precess the spin accumulation into the $[110]$ direction [8,17]. We therefore expect to observe an increase in the current-induced spin accumulation at low fields followed by a suppression due to spin dephasing in large fields. The signal should reverse sign when B_y is reversed or when the contact magnetizations are reversed. The voltage $V_{ab} - V_{cd}$, shown in Fig. 1(c) for the two different magnetization directions on the GaAs sample with a channel current $j_x =$

$5.7 \times 10^3 \text{ A/cm}^2$ at $T = 30 \text{ K}$, shows that the expected behavior is superimposed on a background that remains in spite of the differential measurement. The background is due to (1) imperfect cancellation of the background Hall voltage due to the applied field, (2) imperfect cancellation of local Hall effects due to the fringe fields generated by the FM contacts, and (3) voltages due to the small fraction (0.1%) of the channel current that is shunted through the Fe contacts. We can eliminate the first two effects based on the expected symmetries of the signal. For example, reversing the magnetizations of both Hall contacts from the $+x$ to $-x$ directions reverses the sign of the spin-dependent voltage but not an ordinary Hall voltage, which can therefore be removed by subtracting the data obtained in the two different parallel states. At low applied fields, local Hall effects are due predominantly to the x components of the contact magnetization. The corresponding fringe fields, which are in the $\pm z$ direction are *even* with respect to B_y , while the spin-dependent signal is *odd* in B_y . We can therefore eliminate local Hall effects by retaining only the components of the signal that are odd with respect to B_y .

The data from Fig. 1(c) are shown in Fig. 1(d) after removing the first two backgrounds. By construction, these data are odd with respect to B_y , and they show extrema at intermediate fields (approximately 250 Oe) as expected. The magnitude of the voltage at these maxima corresponds to a spin polarization $P = (n^\uparrow - n_\downarrow)/(n^\uparrow + n_\downarrow) \approx 1.3\%$ at the sample edges, where

$$P = \frac{e\Delta V}{\eta P_{\text{Fe}}} \frac{3m^*}{\hbar^2(3\pi^2n)^{2/3}}. \quad (1)$$

In this expression, which follows from the usual relationship between the spin accumulation and the density of states [16], $P_{\text{Fe}} = 0.42$ is the spin polarization of Fe at the Fermi level and $\eta \sim 0.5$ is the interfacial transparency. There are, however, additional features in the field sweeps near 1 kOe that do not reverse sign when the current is reversed, and hence cannot be due to a Hall effect. These derive from the features (at the same fields) in the data of Fig. 1(c) and result from the current that is shunted through the Fe contacts (and hence has a component perpendicular to the plane) in combination with tunneling anisotropic magnetoresistance (TAMR) at the Schottky contact [18]. This final background contribution can be minimized by subtracting the voltages for the two current directions, as will be done for all subsequent data shown in this Letter.

We have also performed the same measurements with the FM contacts on opposite sides of the channel initialized in either of the antiparallel states $\uparrow\downarrow$ or $\downarrow\uparrow$. The data in this case are shown as the solid line in Fig. 1(d) after removal of all three backgrounds. This curve shows no signal, indicating that the spin accumulations at opposite edges of the sample are opposite in sign.

Data taken at different contact separations for the $x = 0$, 0.03, 0.05 and 0.06 devices at $T = 30 \text{ K}$ and $j_x = \pm 2.9 \times 10^3 \text{ A/cm}^2$ are shown in Fig. 2. The SHE-induced spin

accumulation ΔV has been converted to spin polarization using Eq. (1). The polarization at contacts further from the edges of the channel shows a field dependence that is qualitatively similar to that observed at the edges, but with a smaller magnitude and narrower width. The devices with a nonzero In concentration x show a smaller spin accumulation that decays more rapidly with distance from the edges of the channel. No spin signal is observed 10 μm from the channel edges for $x = 0.03$ or at 6 and 10 μm from the edges for $x = 0.05$ and 0.06. As confirmed by nonlocal measurements, these samples have shorter spin diffusion lengths than the GaAs sample. Data similar to those shown in Fig. 2 were taken over a bias range of $j_x = 0$ to $\pm 5.7 \times 10^3$ A/cm² at $T = 30$ K and a temperature range of $T = 30$ to 200 K at $j_x = \pm 5.7 \times 10^3$ A/cm².

We now use these data to determine the magnitude and sign of the spin Hall conductivity. The transverse spin current $j_s \hat{y}$ is related to the steady-state spin polarization P_0 at the channel edges by the diffusion equation, so that $j_s = eP_0 n L_s / \tau_s$, where τ_s is the spin relaxation time and $L_s = \sqrt{D\tau_s}$ is the spin diffusion length. Determining P_0 requires a full fit of $P(B_y)$ to a model that includes pre-

cession in the applied field, diffusion, and spin relaxation. This is similar to the analysis of nonlocal Hanle measurements [16] after accounting for the perpendicular orientation of the “source” (the spin Hall current) with respect to the detector. As with our fitting of nonlocal Hanle curves, we neglect the effects of fringe fields on the spin dynamics. To constrain the fits, the diffusion constant D is obtained from the channel conductivity σ_{xx} and the carrier density n using the Einstein relation [19], and the g factor for each sample is fixed using the value for GaAs, $g = -0.44$ and the dependence on x determined from the 8×8 Kane model [9,20–22]. We detect the component of the spin accumulation that is parallel to the contact magnetization, which we determine from the known saturation field (~ 1 kOe) and a simple Stoner-Wohlfarth model for a uniaxial magnet. This leaves P_0 and τ_s as the only fitting parameters. For each bias current, a single set of parameters is used to fit the data sets obtained at different distances from the edge of the channel. The fitting results are shown as solid curves in Figs. 2(a)–2(d), and P as a function of position for all four samples is shown in Fig. 2(e). The principal features of the data are captured, including the decrease of the signal and the shift of the extrema towards smaller fields as the Fe contacts are moved towards the center of the channel. The broader Hanle curves observed as the In concentration x increases reflect a decreasing spin relaxation time, consistent with nonlocal Hanle curves obtained on devices from the same wafers.

From the values of P_0 and τ_s determined from these fits, it is possible to determine j_s and the spin Hall conductivity $\sigma_{\text{SH}} = j_s / E_x$. For the GaAs sample, we find $\sigma_{\text{SH}} \approx 3.0 \Omega^{-1} \text{m}^{-1}$, which is of the same order of magnitude as has been estimated from Kerr microscopy measurements [9,13] and is of the same order and sign as has been predicted by theory [5,7]. To make a more extensive comparison, we consider the result of Engel and co-workers [5]:

$$\sigma_{\text{SH}} \approx \frac{2\lambda_{\text{so}}}{(a_B^*)^2} \sigma_{xx} - \frac{2n\lambda_{\text{so}}e^2}{\hbar}, \quad (2)$$

where λ_{so} is the spin-orbit coupling parameter, a_B^* is the effective Bohr radius of an ionized impurity (the source of scattering), and σ_{xx} is the channel conductivity. For GaAs, we use $\lambda_{\text{so}} = 5.3 \text{ \AA}^2$ and $a_B^* = 103 \text{ \AA}$ [5]. At the value of j_x used for the data in Fig. 2, $\sigma_{xx} = 3600 \Omega^{-1} \text{m}^{-1}$, and Eq. (2) gives $\sigma_{\text{SH}} = 2.4 \Omega^{-1} \text{m}^{-1}$, a factor of 20% smaller than experiment.

As can be seen from examination of Eq. (2), there are two expected contributions to the spin Hall conductivity, one of which scales with σ_{xx} [skew scattering (SS)] and a second which is a constant of opposite sign [side jump (SJ)]. It is possible to tune the mobility, and hence σ_{xx} , by approximately 25% by varying the bias current [23]. We find clear evidence for both contributions in the observed dependence of σ_{SH} on σ_{xx} , which is shown in Fig. 3(a). The solid lines in this figure are linear fits, with parameters given in Table I. A negative intercept, indicating the ex-

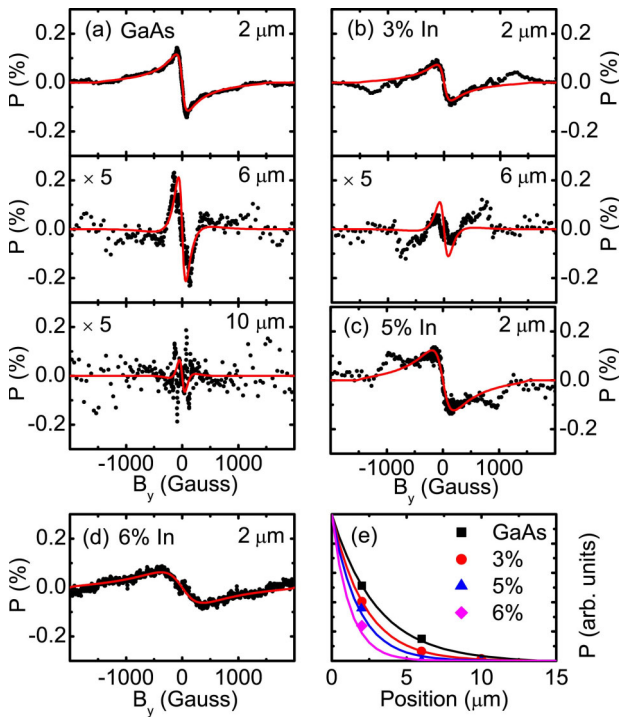


FIG. 2 (color online). (a) SHE-induced polarization P (\bullet) as a function of magnetic field for the GaAs sample at $T = 30$ K and channel current $j_x = \pm 2.9 \times 10^3$ A/cm². The solid curves (—) show fits to all contact separations with a single set of parameters. (b), (c), and (d) Data and fits for the In_xGa_{1-x}As samples for $x = 0.03$ (b), 0.05 (c), and 0.06 (d) under the same bias conditions. No signal was observed for the contact separations that are not shown. (e) Magnitude of the SHE signal as a function of distance from the edge of the channel for all four samples, normalized to P_0 . The solid lines are curves generated from the fitting parameters found in (a)–(d).

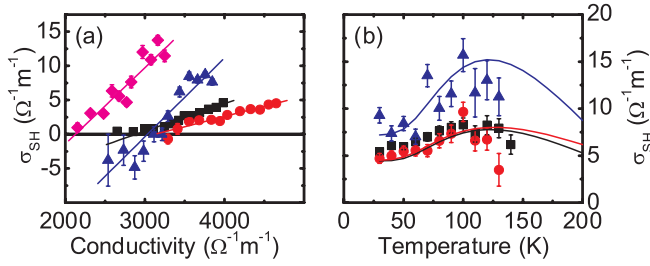


FIG. 3 (color online). (a) Dependence of σ_{SH} on the σ_{xx} at $T = 30$ K for the $x = 0$ (squares), 0.03 (circles), 0.05 (triangles), and 0.06 (diamonds) samples. A linear fit is used to determine γ and σ_{SJ} for each sample. The fitting parameters are compiled in Table I. (b) Temperature dependence of σ_{SH} from $T = 30$ to 130 K (solid points) and predicted temperature dependence (curves).

pected sign of the side-jump term, is found in all four samples. We can write the total spin Hall conductivity as $\sigma_{\text{SH}} = \sigma_{\text{SS}} + \sigma_{\text{SJ}} = \gamma\sigma_{xx} + \sigma_{\text{SJ}}$, where γ and σ_{SJ} are obtained from Eq. (2). The skewness parameter γ for GaAs is about 4 times larger than the prediction of $\sim 1 \times 10^{-3}$ [5]. We can also compare our experimental results with the expected ratio $\sigma_{\text{SJ}}/\gamma = -a_B^* n e^2 \hbar$, which is independent of the spin-orbit coupling λ_{so} . We find that $\sigma_{\text{SJ}}/\gamma$, is about a factor of 2.5 larger than the expected value for all four samples.

We studied the temperature dependence of the SHE in the $x = 0, 0.03$, and 0.05 samples over the range $T = 30$ to 150 K at $j_x = 5.7 \times 10^3$ A/cm². Figure 3(b) shows the experimentally determined spin Hall conductivity as a function of temperature (solid points). The solid lines show the predicted temperature dependence of σ_{SH} using the values of γ and σ_{SJ} determined from Fig. 3(a) and the measured values of $\sigma_{xx}(T)$ and $n(T)$. We find that σ_{SH} shows a modest increase over the temperature range of $T = 30$ to 100 K due to the increase in electron mobility. At temperatures above ≈ 120 K the measured spin accumulation decreases rapidly due to the rapid decrease of τ_s with increasing temperature. This suppresses the spin Hall signal even if σ_{SH} were constant. The weaker temperature dependence of τ_s in other materials, such as ZnSe, makes the SHE more readily observable at high temperatures [12].

The measurements and analysis presented here conclusively demonstrate electrical detection of the direct SHE in Fe/In_xGa_{1-x}As heterostructures. The bias and temperature dependences of the SHE indicate that both skew and side-jump scattering contribute to the total spin Hall conductivity. The ratios of the side-jump to skew scattering contributions for the four samples are similar but larger than predicted for ionized impurity scattering alone. We note that the spin accumulation due to the SHE observed for the higher In concentrations is comparable to that generated by direct spin injection from a ferromagnet. This suggests that

TABLE I. Fit parameters for $\sigma_{\text{SH}} = \gamma\sigma_{xx} + \sigma_{\text{SJ}}$.

x (In concentration)	0.00	0.03	0.05	0.06
$\gamma(10^{-3})$	4	3	12	13
$\sigma_{\text{SJ}}(\Omega^{-1}\text{m}^{-1})$	-12	-9	-35	-28
Meas. $\sigma_{\text{SJ}}/\gamma(10^3\Omega^{-1}\text{m}^{-1})$	-3.0	-3.0	-2.9	-2.2
Pred. $\sigma_{\text{SJ}}/\gamma(10^3\Omega^{-1}\text{m}^{-1})$	-1.1	-1.4	-1.2	0.8

the SHE could function as a tool for probing spin-dependent phenomena in materials with large spin-orbit coupling and short spin diffusion lengths.

We acknowledge helpful discussions with M. E. Flatté. This work was supported by the ONR MURI program and NSF Grant No. DMR-0804244, and in part by the NSF MRSEC program under Grant No. DMR-0819885.

- [1] M. I. D'yakonov and V. I. Perel, *Phys. Lett. A* **35**, 459 (1971).
- [2] S. Murakami, N. Nagaosa, and S.-C. Zhang, *Science* **301**, 1348 (2003).
- [3] J. Sinova *et al.*, *Phys. Rev. Lett.* **92**, 126603 (2004).
- [4] J. Schliemann and D. Loss, *Phys. Rev. B* **69**, 165315 (2004).
- [5] H.-A. Engel, B. I. Halperin, and E. I. Rashba, *Phys. Rev. Lett.* **95**, 166605 (2005).
- [6] B. A. Bernevig and S.-C. Zhang, *Phys. Rev. B* **72**, 115204 (2005).
- [7] W. K. Tse and S. Das Sarma, *Phys. Rev. Lett.* **96**, 056601 (2006).
- [8] H.-A. Engel, E. I. Rashba, and B. I. Halperin, *Phys. Rev. Lett.* **98**, 036602 (2007).
- [9] Y. K. Kato, R. C. Myers, A. C. Gossard, and D. D. Awschalom, *Science* **306**, 1910 (2004).
- [10] J. Wunderlich, B. Kaestner, J. Sinova, and T. Jungwirth, *Phys. Rev. Lett.* **94**, 047204 (2005).
- [11] V. Sih *et al.* *Nature Phys.* **1**, 31 (2005).
- [12] N. P. Stern *et al.*, *Phys. Rev. Lett.* **97**, 126603 (2006).
- [13] S. Matsuzaka, Y. Ohno, and H. Ohno, *Phys. Rev. B* **80**, 241305(R) (2009).
- [14] J. Wunderlich *et al.*, *Nature Phys.* **5**, 675 (2009).
- [15] C. Brune *et al.*, *Nature Phys.* **6**, 448 (2010), and references therein.
- [16] X. Lou *et al.*, *Nature Phys.* **3**, 197 (2007).
- [17] S. A. Crooker *et al.*, *Science* **309**, 2191 (2005).
- [18] J. Moser *et al.*, *Phys. Rev. Lett.* **99**, 056601 (2007).
- [19] M. E. Flatté and J. M. Byers, *Phys. Rev. Lett.* **84**, 4220 (2000).
- [20] E. A. de Andrada e Silva, G. C. La Rocca, and F. Bassani, *Phys. Rev. B* **55**, 16293 (1997).
- [21] A. A. Kiselev, E. L. Ivchenko, and U. Rössler, *Phys. Rev. B* **58**, 16353 (1998).
- [22] *Semiconductors-Basic Data* edited by O. Madelung (Springer, New York, 1996).
- [23] D. J. Oliver, *Phys. Rev.* **127**, 1045 (1962).